PCT WORLD INTELLECTUAL PROPERTY ORGANIZATION
International Bureau

INTERNATIONAL APPLICATION PUBLISHED UNDER THE PATENT COOPERATION TREATY (PCT)

(51) International Patent Classification 6 : G01B 7/00, G01D 5/14, G01P 3/46	A1	(11) International Publication Number: WO 00/14476
		(43) International Publication Date: 16 March 2000 (16.03.00)

(21) International Application Number: PCT/AU99/00733

(22) International Filing Date: 7 September 1999 (07.09.99)

(30) Priority Data:

PP 5702	7 September 1998 (07.09.98)	AU
PP 7709	14 December 1998 (14.12.98)	AU

(71)(72) Applicant and Inventor: MICHALEWICZ, Marek, Tadeusz [AU/AU]; 112 Rankins Road, Kensington, VIC 3031 (AU).

(74) Agents: NOONAN, Greg et al.; Freehills Patent Attorneys, Level 47, 101 Collins Street, Melbourne, VIC 3000 (AU).

(81) Designated States: AE, AL, AM, AT, AU, AZ, BA, BB, BG, BR, BY, CA, CH, CN, CR, CU, CZ, DE, DK, DM, EE, ES, FI, GB, GD, GE, GH, GM, HR, HU, ID, IL, IN, IS, JP, KE, KG, KP, KR, KZ, LC, LK, LR, LS, LT, LU, LV, MD, MG, MK, MN, MW, MX, NO, NZ, PL, PT, RO, RU, SD, SE, SG, SI, SK, SL, TJ, TM, TR, TT, UA, UG, US, UZ, VN, YU, ZA, ZW, ARIPO patent (GH, GM, KE, LS, MW, SD, SL, SZ, UG, ZW), Eurasian patent (AM, AZ, BY, KG, KZ, MD, RU, TJ, TM), European patent (AT, BE, CH, CY, DE, DK, ES, FI, FR, GB, GR, IE, IT, LU, MC, NL, PT, SE), OAPI patent (BF, BJ, CF, CG, CI, CM, GA, GN, GW, ML, MR, NE, SN, TD, TG).

Published
With international search report.

(54) Title: MEASUREMENTS USING TUNNELLING CURRENT BETWEEN ELONGATE CONDUCTORS

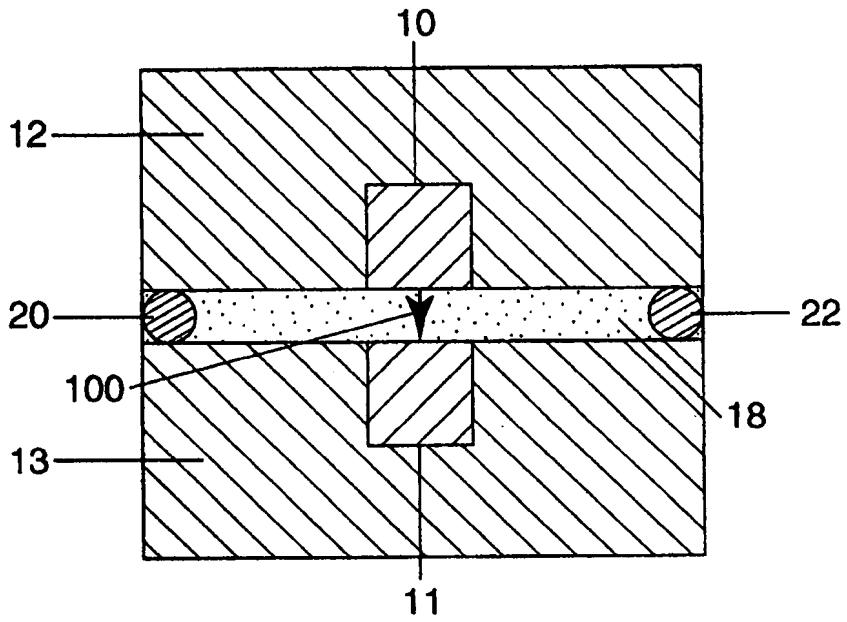

(57) Abstract

Apparatus for use in measuring and/or monitoring the relative position or displacement of two elements, includes a pair of elongate electrical conductors (10, 11) adapted to be associated with the respective elements, and means (12, 13, 18) for disposing the conductors at a mutual separation such that a detectable quantum tunnelling current may be generated between them on application of an electrical potential difference between the conductors.

FOR THE PURPOSES OF INFORMATION ONLY

Codes used to identify States party to the PCT on the front pages of pamphlets publishing international applications under the PCT.

AL	Albania	**ES**	Spain	**LS**	Lesotho	**SI**	Slovenia
AM	Armenia	**FI**	Finland	**LT**	Lithuania	**SK**	Slovakia
AT	Austria	**FR**	France	**LU**	Luxembourg	**SN**	Senegal
AU	Australia	**GA**	Gabon	**LV**	Latvia	**SZ**	Swaziland
AZ	Azerbaijan	**GB**	United Kingdom	**MC**	Monaco	**TD**	Chad
BA	Bosnia and Herzegovina	**GE**	Georgia	**MD**	Republic of Moldova	**TG**	Togo
BB	Barbados	**GH**	Ghana	**MG**	Madagascar	**TJ**	Tajikistan
BE	Belgium	**GN**	Guinea	**MK**	The former Yugoslav Republic of Macedonia	**TM**	Turkmenistan
BF	Burkina Faso	**GR**	Greece			**TR**	Turkey
BG	Bulgaria	**HU**	Hungary	**ML**	Mali	**TT**	Trinidad and Tobago
BJ	Benin	**IE**	Ireland	**MN**	Mongolia	**UA**	Ukraine
BR	Brazil	**IL**	Israel	**MR**	Mauritania	**UG**	Uganda
BY	Belarus	**IS**	Iceland	**MW**	Malawi	**US**	United States of America
CA	Canada	**IT**	Italy	**MX**	Mexico	**UZ**	Uzbekistan
CF	Central African Republic	**JP**	Japan	**NE**	Niger	**VN**	Viet Nam
CG	Congo	**KE**	Kenya	**NL**	Netherlands	**YU**	Yugoslavia
CH	Switzerland	**KG**	Kyrgyzstan	**NO**	Norway	**ZW**	Zimbabwe
CI	Côte d'Ivoire	**KP**	Democratic People's Republic of Korea	**NZ**	New Zealand		
CM	Cameroon			**PL**	Poland		
CN	China	**KR**	Republic of Korea	**PT**	Portugal		
CU	Cuba	**KZ**	Kazakstan	**RO**	Romania		
CZ	Czech Republic	**LC**	Saint Lucia	**RU**	Russian Federation		
DE	Germany	**LI**	Liechtenstein	**SD**	Sudan		
DK	Denmark	**LK**	Sri Lanka	**SE**	Sweden		
EE	Estonia	**LR**	Liberia	**SG**	Singapore		

MEASUREMENTS USING TUNNELLING CURRENT BETWEEN ELONGATE CONDUCTORS

Field of Invention

This invention relates to the accurate measurement and monitoring of fine relative positions or displacements, eg. rotational or angular separations or displacements, vibrations, linear separations or translations, alignments and misalignments. Of particular, though not exclusive, interest is measurement of angles.

Background Art

Known devices designed for ultra precise measurement of angles include autocollimators, diffraction based systems and gears based systems. Autocollimators use measurement of angular deviation to determine in turn, eg, straightness, flatness, squareness and parallelism. Modern forms use laser diode light sources and beamsplitters, and incorporate a micrometer in the eyepiece viewing system for accurate measurement of angular displacement. Typical best accuracies are 0.2 arcseconds, for a measuring range of 160 arcseconds.

In a known goniometer-style instrument, a pair of radial gratings rotate in unison at a uniform speed and are scanned by a pair of reading heads. One of these is stationary while the other moves through the angle to be measured. The relative phase change between the two resultant signals is an indication of the rotation of the moveable reading head with respect to the fixed head. Accuracy achieved is said to be 0.1 arcsecond.

These prior devices are relatively expensive and typically rather large instruments. Often they form a key part of another scientific apparatus, such as a diffractemeter, where the precise measure of angle determines the resolution and quality of an instrument.

Accuracy of angular measurement is the subject of Zhang et al. "Improving the Accuracy of Angle Measurement System with Optical Grating", Annals of the

CIRP Vol 43, No. 1 (1994). This paper proposes the use of index gratings with sine function transmissivity, and other enhancements, and reports an accuracy of 0.2 arcseconds with a prototype instrument.

It is an object of this invention to provide for fine measurement and monitoring of relative positions or displacements, whether angular, linear or otherwise, to a satisfactory accuracy that is preferably better than that achieved with known instruments and techniques.

Summary of the Invention

The invention proposes an approach quite different from that previously used, and entails monitoring the quantum tunnelling current between two proximate electrical conductors, preferably of nano dimensions. In a preferred embodiment, two arrays of aligned conductors may be used, and these may advantageously be carbon nanotubes.

The invention accordingly provides, in a first aspect, a method of measuring and/or monitoring the relative position or displacement of two elements, including:

associating the elements with respective elongate electrical conductors;

disposing the conductors preferably in approximate alignment, at a mutual separation and applying an electrical potential difference such that there is a detectable quantum tunnelling current between them; and

detecting and/or measuring said quantum tunnelling current.

Preferably, the relative positions of the conductors is adjusted to determine that position at which maximum quantum tunnelling current is detected.

In a second aspect, the invention provides apparatus for use in measuring and/or monitoring the relative position or displacement of two elements. The apparatus includes a pair of elongate electrical conductors adapted to be associated with the respective elements, and means for disposing the conductors,

preferably substantially aligned in mutually parallel relationship, at a mutual separation such that a detectable quantum tunnelling current may be generated between them on the application of an electrical potential difference between the conductors.

The apparatus may further include means to apply said potential difference, and means to detect and/or measure the quantum tunnelling current between the conductors.

Preferably, the apparatus further includes means to adjust the relative positions of the conductors to determine that position at which maximum quantum tunnelling current is detected.

The position or displacement may be one or more of a rotational or angular separation or displacement, a vibration, a linear separation or translation, an alignment and a misalignment.

Preferably, the electrical conductors are of width 1 micron or less eg, in one or more embodiments, of width in the nano-order to sub-micron range. In the latter case, the conductors may be carbon nanotubes of arbitrary helicity or radius, either single or multi-walls of carbon monofilaments, or nanowires. Alternatively, the conductors may be, eg, micron to sub-micron quasi one-dimensional conductors. In some embodiments, the conductors may be of length 1 mm or less.

The conductors may be associated with the aforesaid elements by being mounted in or on an insulating or semiconducting substrate, preferably flush with a surface of the substrate. The substrate may be, eg. a solid or a crystal face. The conductors may be placed along respective atomic steps on a vicinal surface.

Advantageously, the electrical conductors are arranged in respective ordered grids or arrays of electrical conductor segments, preferably wired in parallel e.g. through a single supply lead, which grids or arrays are complementary and overlaid to place the conductor segments in sufficient proximity to obtain detectable quantum tunnelling currents.

Brief Description of the Drawings

The invention will now be further described, by way of example only, with respect to the accompanying drawings, in which:

Figure 1 is a fragmentary cross-section of a first embodiment of nano-dimension device according to the invention, with the respective conductors generally aligned and electrical connections diagrammatically depicted;

Figure 2 is a modification of the embodiment of Figure 1 in which the conductors are substantially at right angles;

Figure 3 is a view similar to Figure 1 of an embodiment that utilises multiple nanotube conductors;

Figure 4 is a view similar to Figure 2 of a modification of the embodiment of Figure 3;

Figure 5 depicts a variation of the embodiment of Figure 3, formed in a particular manner; and

Figure 6 is a view similar to Figures 1 and 3 of a further embodiment of the invention that utilises an etched conductive overlay and a film applied by Langmuir-Blodgett technology.

In the embodiment of Figure 1, respective nano-dimension elongate electrically conductive wires 10, 11, of widths in the nano to sub-micron dimension range, are embedded flush in respective insulating medium substrates 12, 13. In this case, the wires are superposed in substantially aligned parallel relationship, at a separation or gap 18 in the range 2-50 Angstroms, such that when an electrical potential difference is applied by a potential source 26 across the conductors, there is a quantum tunnelling current 100 between them detectable in suitable detection circuit 27.

A suitable technique for making the embodiment is electron beam nanolithography, in which aligned conducting wire can be delineated on a semi-conducting substrate. This is described, eg. in Wilkinson et al, "Electron Beam Nanolithography", an article in the text "The Physics and Fabrication of Microstructures and Microdevices" (eds. Kelly & Weisbuch, Spring-Verlag, 1986) that describes and illustrates a set of parallel GaAs conducting wires on a semi-insulating substrate. In practical applications of the device, substrates or plates 12, 13 are associated or coupled to respective elements whose displacement or position is to be measured or monitored.

In general, tunnelling current 100 is proportional to the product of the local densities of states on a pair of adjacent electrodes (ie. conductors), or in other terms, to the sum of the square of the tunnelling matrix elements between states on both electrodes. It is also a sensitive function of the tunnelling potential and the electrode curvature. Furthermore, quantum tunnelling current is critically dependent on the spacing between the conductors because the quantum wave function decays exponentially outside the conductor surface, and the detected current will be a function of the relative angle between a pair of crossed nanotubes. The invention takes advantage of the aforementioned exponential and angular relationship in that the detected value of the tunnelling current 100 will change sharply as the longitudinal opposed surface segments of the conductor move apart with increasing rotational and/or translational misalignment or vice versa.

More particularly, suitable Schrodinger wave functions for the gap 18 are found in Kiejna & Wojciechowski, "Metal Surface Electron Physics", Pergamon (1996). It could be demonstrated from wave function analysis that the quantum tunnelling current is critically dependent on the spacing between the conductors because the quantum wave function decays exponentially outside the conductor surface, and the detected current will also be a function of the relative angle between a pair of crossed nanoconductors.

The gap 18 between the aligned opposed conductor surface segments is thought to be most appropriately in the range 2-50 Angstroms, more preferably 2-

20 Angstroms. The conductor segments may conveniently be of any length that can practicably be placed and aligned on the substrate and have leads attached, eg. in the range 1μ to 10^{-2}m long.

Gap 18 may be a partial vacuum or may be filled with an appropriate medium. Suitable arrangements for accurately maintaining the gap 18 include the use of buckyball (C_{60}) nanobearings 20, 22, or the interpositioning of a separation film of an organic medium, preferably an organic lubricant eg. cyclohexane (further disclosed below). The latter is thought to be a particularly effective approach to the maintenance of accurately parallel fine separation.

The adjustment means may include piezoelectric positioners of known type suitable for performing adjustments at nano dimension level.

The aforementioned effect is further enhanced if the conductors are cylindrical, as for carbon nanotubes. In the case of the grids or arrays if the conductor segments are connected in parallel, there will be an amplifying effect and this will facilitate current measurement. However, if the lines have independent connections, the grids forming the sandwich will be able to act as two dimensional arrays of point "capacitors" which can be switched on and off independently, forming a "pixelised" array of tunnelling wells.

The tunnelling current 100 will exhibit minima at one or more positions dependent on the aspect ratio (length to separation of conductor segments), and a maximum when the conductor segments of the two grids/arrays are perfectly aligned.

Figure 3 illustrates an alternative embodiment in which the electrical conductors comprise multiple parallel nanotubes 10a, 10b, 10c, 11a, 11b, 11c deposited on insulating medium substrates 12', 13'.

Procedures for producing a set of aligned nanotubes on a substrate are described, for example, at Chauvet et al, Physical Review B**52**, 52 (1995); de

Heer et al, Science **268**, 845 (1995); and Kiang et al, Carbon **33**, 903-914 (1995).

The properties of single wall nanotubes are described, for example, in Iijima, Nature **354**, 56-58 (1991) and Iijima et al, Nature **363**, 603-605 (1993). Carbon nanotubes of a variety of types are also described at Östling et al, Physical Review B. **55**, 55 (1997).

A particular technique for producing a grid of parallel conductor segments suitable for this invention is by epitaxial deposition of nanotubes or other nano-dimension conductors on the atomic steps of a vicinal surface produced by slicing a crystal at an angle to a primary plane. The separation of the conductor segments may be regular or irregular, but is most preferably parallel. Figure 5 shows a modification of the embodiment of Figure 3 in which the nanotubes are deposited in this way at the successive atomic steps 14, 15 on a stepped vicinal surface.

Figures 2 and 4 illustrate embodiments in which the respective arrays of conductors of micron, submicron or nano-order dimensions when not nanotubes, are arranged with the conductors 210 of one array in or on substrate 212, extending substantially at right angles to the conductors 211 of the other array, in or on substrate 213. Instead of a right angle, the angular relationship may be at some other angle, eg. to form a diamond or rhomboidal type of two dimensional lattice. In one application of such an arrangement preferably utilising a large number of conductor lines, the set of cross-over points 250 will form an artificial scattering lattice effective to scatter a beam of atoms directed parallel to the sandwich structure into the space 218 between the conductor arrays. If each line is independently electrically connected, ie they are not electrically in parallel, there will be a pixellised array which is an analog of a two-dimensional "pinball game" for atoms, with predefined scattering centres.

In a variation of the scattering lattice, it may further include an array of magnetic elements forming the lattice and creating 1-dimensional domains at or between the cross-over points.

Figure 6 is a further embodiment in which each substrate 312, 313 is atomically smooth freshly cleaved mica, and the conductors 310, 311 are formed by etching an overlay 330, 331 of gold, and then filling the interstial grooves by application of a molecular monolayer by a Langmuir-Blodgett process. The two arrays may be separated as before by a cyclohexane or other suitable organic lubricant film 318 maintained by an outer thermoshrink wrap 340.

The illustrated devices are effective electro-mechanical nanodevices. On the one hand, they may be applied to the measurement of angles, angles of rotation, rotational speed, and alignment or misalignment at microscopic and macroscopic level. Rotational speed can be measured, for example, by measuring the number of current maxima per unit of time. It is thought to be capable of an accuracy of the order of 0.01 arcseconds over an operational angular range of 20° or so.

Alternatively, the illustrated devices may be used for measuring or monitoring relative linear position or translation. If one substrate in the embodiments of Figures 3, 5 and 6 is translated with respect to the other, there will be a series of very sharp peaks observed in tunnelling current 100. The distance traversed will be given by the number of observed peaks times the separation between the conductors; the resolution will be of the order of the width of the conductors, i.e. about 200 Angstroms with currently available nanolithography technology, but about 10-30 Angstroms with nanotubes.

The rotational and translational effects would both contribute to vibration monitoring or measurement, eg. in a seismograph.

CLAIMS

1. Apparatus for measuring and/or monitoring the relative position or displacement of two elements, including:

a pair of elongate electrical conductors adapted to be associated with the respective elements; and

means for disposing the conductors at a mutual separation such that a detectable quantum tunnelling current may be generated between them on application of an electrical potential difference between said conductors.

2. Apparatus according to claim 1, further including means to adjust the relative positions of the conductors to determine that position at which maximum quantum tunnelling current is detected.

3. Apparatus according to claim 2 wherein said adjustment means includes one or more piezoelectric positioners.

4. Apparatus according to any claim 1, 2 or 3 wherein said elongate electrical conductors are substantially aligned in mutually parallel relationship.

5. Apparatus according to any preceding claim, wherein said elongate electrical conductors are arranged in respective ordered grids or arrays of electrical conductor segments, which grids or arrays are complementary and overlaid to place the conductor segments in sufficient proximity to obtain detectable quantum tunnelling currents.

6. Apparatus according to claim 5 wherein the conductor segments of each said grid or array are substantially parallel but aligned at an angle to the conductor segments of the other grid(s) or array(s).

7. Apparatus according to claim 5 or 6 wherein the conductor segments of each grid or array are wired electrically in parallel.

8. Apparatus according to any preceding claim wherein said elongate electrical conductors are of micron to nano-order dimensions.

9. Apparatus according to claim 8 wherein said elongate electrical conductors are carbon nanotubes or nanowires, or micron to sub-micron quasi one dimensional conductors.

10. Apparatus according to any preceding claim wherein said conductors are associated with the aforesaid elements by being mounted in or on respective insulating or semiconductive substrates.

11. Apparatus according to claim 9 where said conductors are flush with a surface of the respective substrates.

12. Apparatus according to any preceding claim wherein each said electrical conductor is disposed along a respective atomic step on a vicinal surface providing a substrate.

13. Apparatus according to any one of claims 1 to 8 wherein said elongate electrical conductors comprise respective segments of an integral conductive layer on an insulating or semiconductive substrate.

14. Apparatus according to claim 13, wherein said segments are separated and/or overlaid by a membrane or film of insulating medium.

15. Apparatus according to any preceding claim wherein said mutual separation of opposed surface segments of said electrical conductors is in the range 2-50 Angstroms.

16. Apparatus according to any preceding claim wherein said mutual separation of opposed surface segments of said electrical conductors is in the range of 2-20 Angstroms.

17. Apparatus according to any preceding claim, wherein said conductors are in one or more conductor segments of length in the range 10^{-6} to 10^{-2}m.

18. Apparatus according to any preceding claim, wherein said means for disposing said conductors at said mutual separation includes an intervening film and means to confine said film.

19. Apparatus according to claim 18 where said intervening film is a film of an organic medium, eg an organic solvent.

20. Apparatus according to any preceding claim, wherein said means for disposing said conductors at said mutual separation includes nanutube or buckyball (C_{60}) bearings.

21. Apparatus according to any preceding claim, wherein said position or displacement measured and/or monitored is one or more of a rotational or angular separational displacement, a vibration, a linear separation or translation, an alignment and a misalignment.

22. Apparatus according to any preceding claim, said elongate electrical conductors are arranged in respective ordered grids or arrays of electrical conductor segments, whereby the cross-over points of the respective arrays define a lattice of electrostatic scattering wells.

23. Apparatus according to claim 22, wherein said lattice further includes an array of magnetic elements forming the lattice and creating 1-dimensional domains at or between said cross-over points.

24. Apparatus according to any one of claims 1 to 23 further including means to apply said electrical potential difference, and means to detect and/or measure said quantum tunnelling current between said conductors.

25. A method of measuring and/or monitoring the relative position or displacement of two elements, including:

associating the elements with respective elongate electrical conductors;

disposing the conductors at a mutual separation and applying to the conductors an electrical potential difference such that there is a detectable quantum tunnelling current between them; and

detecting and/or measuring said quantum tunnelling current.

26. A method according to claim 24, further including adjusting the relative positions of the conductors to determine one or more positions at which maximum quantum tunnelling current is detected.

FIGURE 1

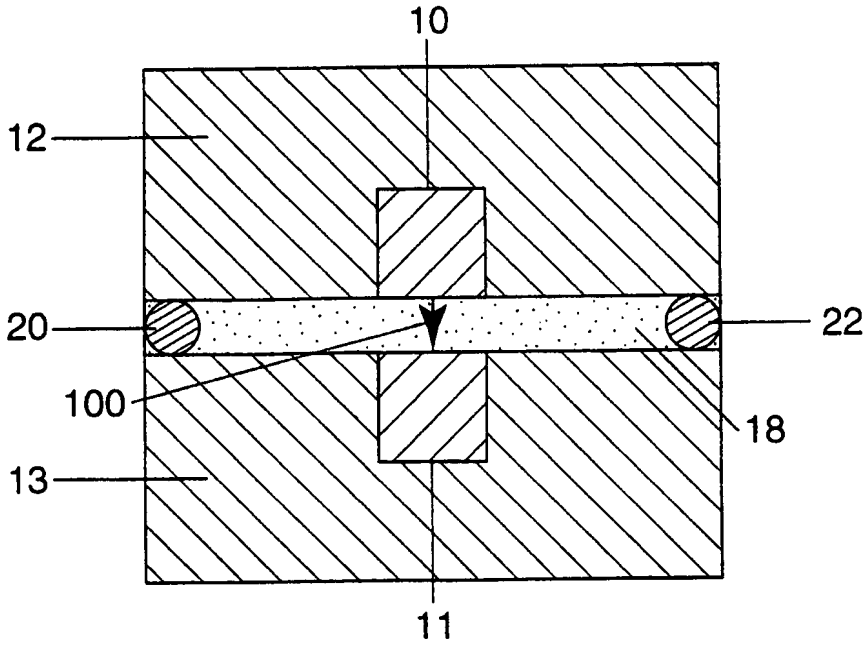

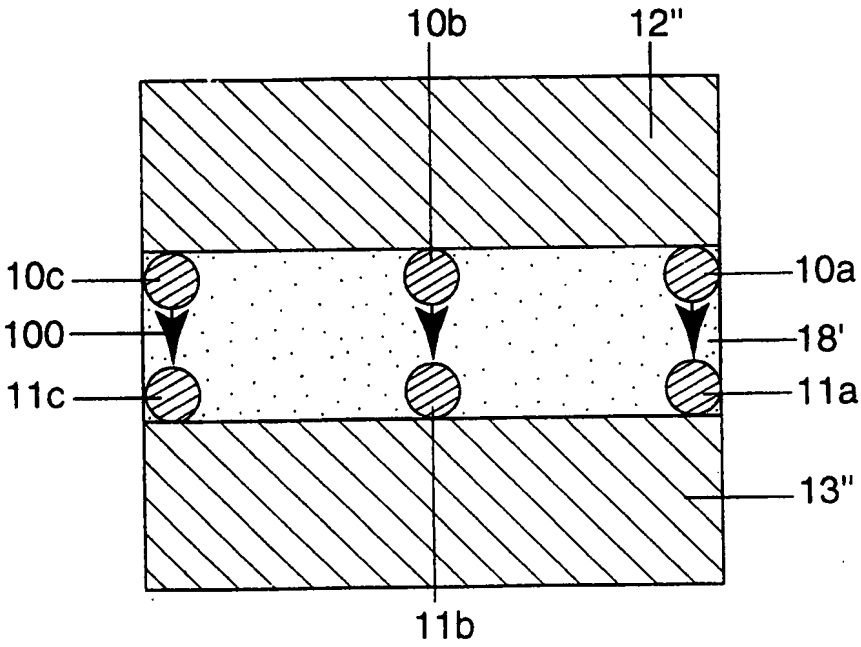

FIGURE 3

FIGURE 2

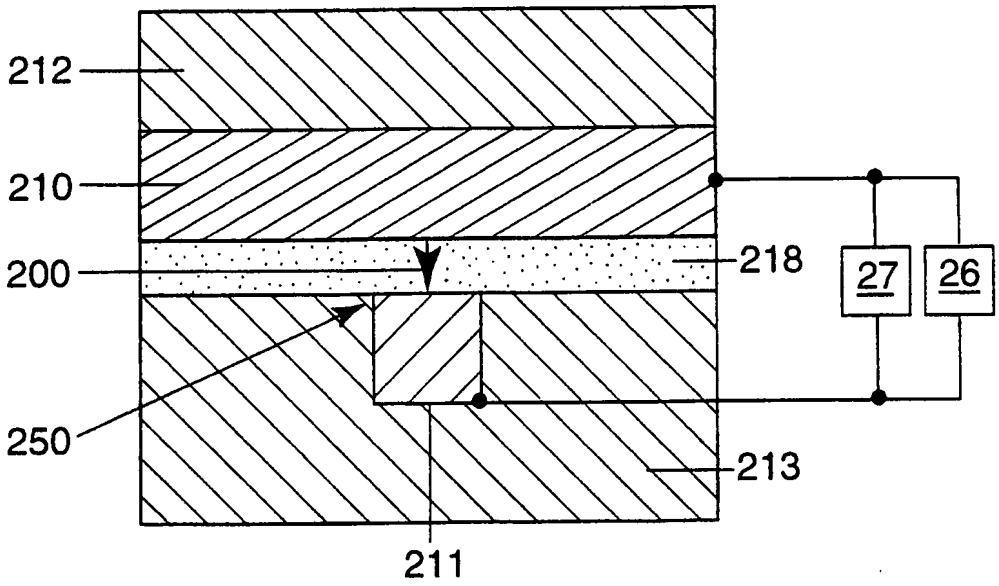

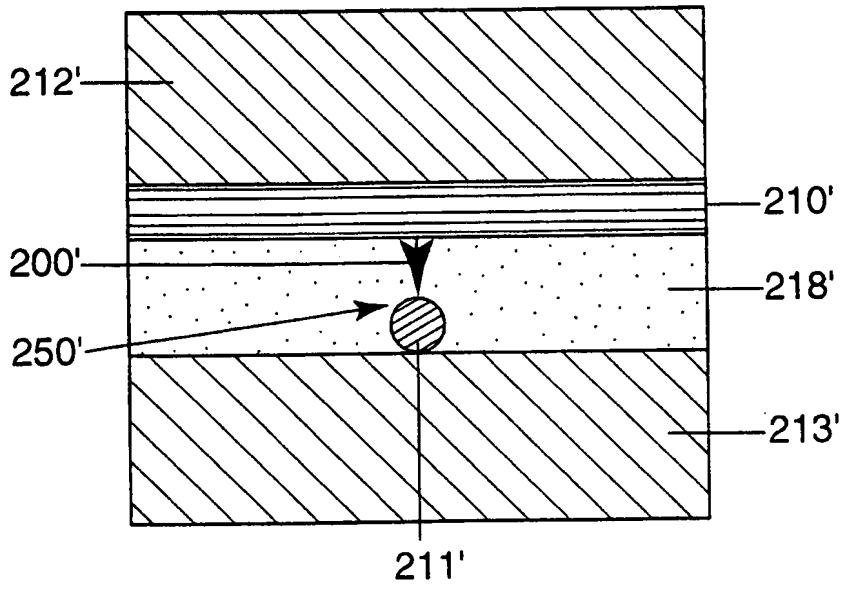

FIGURE 4

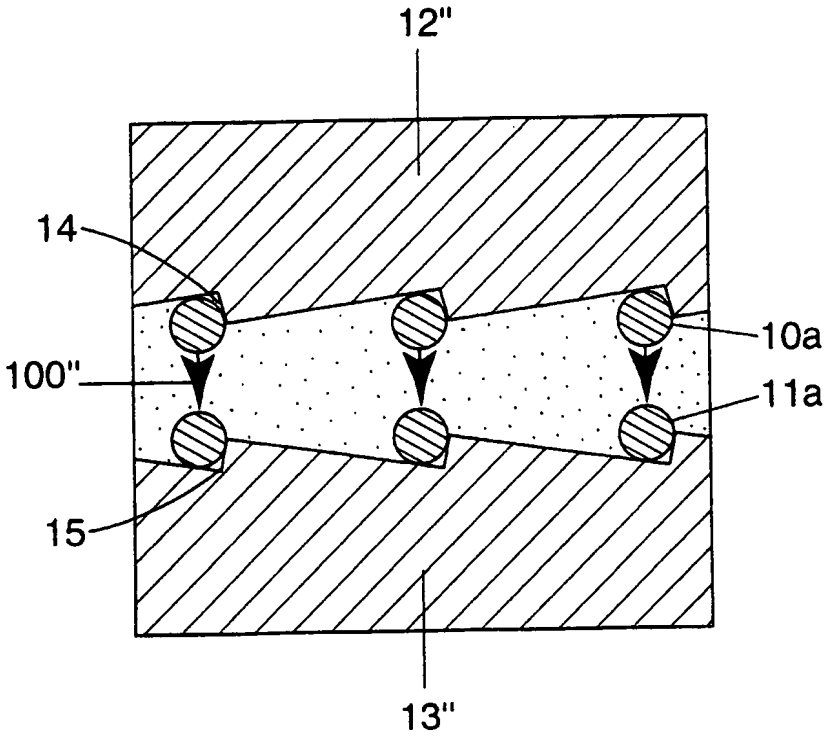

FIGURE 5

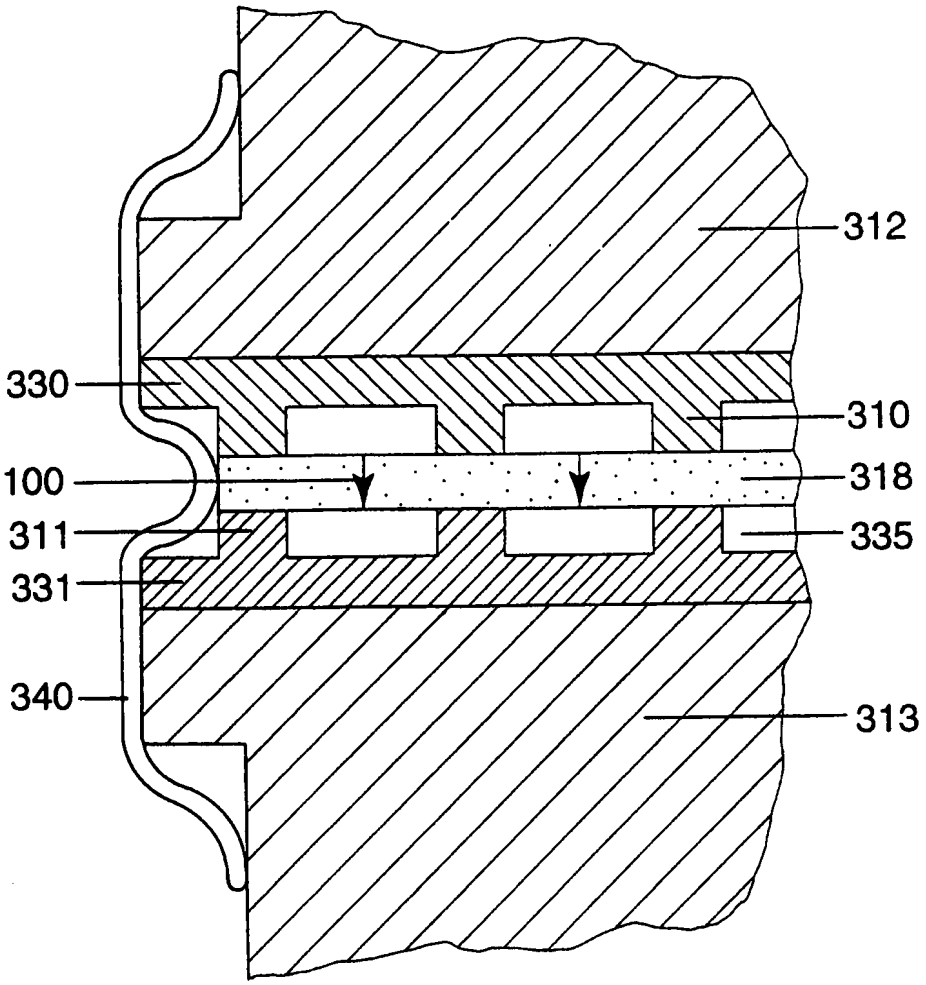

FIGURE 6

INTERNATIONAL SEARCH REPORT

International application No.
PCT/AU 99/00733

A. CLASSIFICATION OF SUBJECT MATTER

Int. Cl.[6]: G01B 7/00, G01D 5/14, G01P 3/46

According to International Patent Classification (IPC) or to both national classification and IPC

B. FIELDS SEARCHED

Minimum documentation searched (classification system followed by classification symbols)
Int. Cl.[6]: G01B 7/-, G01C 1/-, G01D 5/-, G01H 1/-, 11/-, G01P 3/-

Documentation searched other than minimum documentation to the extent that such documents are included in the fields searched

Electronic data base consulted during the international search (name of data base and, where practicable, search terms used)
WPAT, JPAT, USPM - Int. Cl.[6] as above with current#, quantum, nano:, buck:, fuller:, c60, micro:, align:, rotat:, angle#, angular, displacement, position, tunnel:

C. DOCUMENTS CONSIDERED TO BE RELEVANT

Category*	Citation of document, with indication, where appropriate, of the relevant passages	Relevant to claim No.
X	US 5756895 A (KUBENA et al.) 26 May 1998 Column 7, lines 19 - 63; figure 4	1, 21, 24, 25
X	US 5679888 A (TOHDA et al.) 21 October 1997 Column 7, line 55 - column 9, line 8; figures 3, 5, 7	1, 21, 24, 25
X	WO 96/21157 A1 (LYNXVALE LIMITED) 11 July 1996 Page 5, lines 9 - 28; page 10, lines 24 - 34; figures 1a, 1b, 8e	1, 21, 24, 25

[X] Further documents are listed in the continuation of Box C

[X] See patent family annex

* Special categories of cited documents:

"A" document defining the general state of the art which is not considered to be of particular relevance

"E" earlier application or patent but published on or after the international filing date

"L" document which may throw doubts on priority claim(s) or which is cited to establish the publication date of another citation or other special reason (as specified)

"O" document referring to an oral disclosure, use, exhibition or other means

"P" document published prior to the international filing date but later than the priority date claimed

"T" later document published after the international filing date or priority date and not in conflict with the application but cited to understand the principle or theory underlying the invention

"X" document of particular relevance; the claimed invention cannot be considered novel or cannot be considered to involve an inventive step when the document is taken alone

"Y" document of particular relevance; the claimed invention cannot be considered to involve an inventive step when the document is combined with one or more other such documents, such combination being obvious to a person skilled in the art

"&" document member of the same patent family

Date of the actual completion of the international search
15 November 1999

Date of mailing of the international search report
9 NOV 1999

Name and mailing address of the ISA/AU
AUSTRALIAN PATENT OFFICE
PO BOX 200
WODEN ACT 2606
AUSTRALIA
Facsimile No.: (02) 6285 3929

Authorized officer

RAJEEV DESHMUKH
Telephone No.: (02) 6283 2145

INTERNATIONAL SEARCH REPORT

International application No.
PCT/AU 99/00733

C (Continuation). DOCUMENTS CONSIDERED TO BE RELEVANT

Category*	Citation of document, with indication, where appropriate, of the relevant passages	Relevant to claim No.
	WO 97/20189 A1 (SMITHS INDUSTRIES PUBLIC LIMITED COMPANY) 5 June 1997	
X	Whole document	1, 21, 24, 25
	EP 646913 A2 (CANON KABUSHIKI KAISHA) 5 April 1995	
A	Whole document	

INTERNATIONAL SEARCH REPORT
Information on patent family members

International application No.
PCT/AU 99/00733

This Annex lists the known "A" publication level patent family members relating to the patent documents cited in the above-mentioned international search report. The Australian Patent Office is in no way liable for these particulars which are merely given for the purpose of information.

Patent Document Cited in Search Report		Patent Family Member					
US	5756895	US	5905202				
US	5679888	EP	706052	JP	9018070		
WO	96/21157	EP	800651	JP	11500528	US	5939632
WO	97/20189	AU	76317/96	EP	864074		
EP	646913	DE	3854173	DE	3856296	EP	304893
		JP	2051018	US	5519686	US	5721721
		JP	2050333	JP	2050332	CA	1328131
		JP	1150813	JP	1147318	JP	1147317
		JP	1053364	JP	1053363		

END OF ANNEX

Stress-induced fragmentation of multiwall carbon nanotubes in a polymer matrix

H. D. Wagner,[a] O. Lourie, Y. Feldman, and R. Tenne
Department of Materials and Interfaces, The Weizmann Institute of Science, Rehovot 76100, Israel

(Received 17 September 1997; accepted for publication 11 November 1997)

We report the observation of single nanotube fragmentation, under tensile stresses, using nanotube-containing thin polymeric films. Similar fragmentation tests with single fibers instead of nanotubes are routinely performed to study the fiber-matrix stress transfer ability in fiber composite materials, and thus the efficiency and quality of composite interfaces. The multiwall nanotube-matrix stress transfer efficiency is estimated to be at least one order of magnitude larger than in conventional fiber-based composites. © *1998 American Institute of Physics.* [S0003-6951(98)03802-9]

Recent experimental and theoretical results[1–7] regarding mechanical properties suggest that carbon nanotubes hold great promise as a possible reinforcing phase in composite materials of a new kind. The bending stiffness of individual carbon nanotubes was shown to be in the 1–5 TPa range,[3,4,8] and techniques are being devised to produce thin films comprising aligned carbon nanotubes.[9] Such developments still present, however, enormous practical challenges, in particular, when probing the properties of individual nanotubes,[3,10–12] for which most studies consist of computer simulations.[2,8] Here, we report the observation of single nanotube fragmentation, under tensile stresses, using nanotube-containing thin polymeric films. Similar fragmentation tests with single fibers instead of nanotubes are routinely performed to study the fiber-matrix stress transfer ability in fiber composite materials, and thus the efficiency and quality of composite interfaces. As will be seen, the multiwall nanotube-matrix stress transfer efficiency is estimated to be at least one order of magnitude larger than that measured in conventional fiber-based composites. It is suggested that the strength of nanotube–polymer interfaces ensues from a photoinduced "2+2" cycloaddition reaction demonstrated earlier in C_{60} photopolymerization.[13,14]

Multiwall carbon nanotubes, prepared by a carbon-arc discharge method (MER Corporation), were sonicated in ethanol and subsequently dried and dispersed on a glass surface. A liquid polymer mixture (urethane/diacrylate oligomer EBECRYL 4858, Radcure Products, UBC Chemicals) was carefully spread onto the dried nanotube-containing graphite powder using a blade, which brought the liquid film down to a thickness of approximately 200 μm. The film was subsequently polymerized for 2 min by means of a Mini-Conveyor UV-Curing Unit (UV process Supply, Inc.), using a 300 W/in. UV lamp. This procedure produced a rigid amorphous polymer film, which was cut into rectangular specimens. These were tested under tension using a Instron 4502 apparatus at a crosshead speed of 50 μm/min. The Young's modulus, strength, and failure strain of the films were 2 GPa, 60 MPa, and 0.075, thus rather similar to high-performance epoxy resins commonly used as matrices in composites. Following mechanical testing, the polymer film was microtomed into thin (70 nm) slices in a direction parallel to the film surface, using a diamond knife and a Reichert–Jung Ultracut microtome (at room temperature). Some polymer films, which had not been mechanically deformed, were also microtomed for comparison. Both types of slices were then examined by transmission electron microscopy (TEM) using a Philips EM 400T at 100 kV. Observation of the nanotubes is made particularly difficult by the presence (and thickness) of the polymer, which strongly reduces the image contrast. The orientation of the nanotubes relative to the direction of tensile deformation was determined by comparison with the traces of the diamond knife in the polymer film during cutting.

The TEM observations reveal that nanotubes that are approximately parallel to the direction of testing undergo a progressive fragmentation process [Figs. 1(a)–1(c)], similar to the single-fiber fragmentation phenomenon observed in macroscopic single-fiber composites.[15,16] The smooth dark damage lines in the nanotubes are believed to be breaks, although only atomic resolution work would fully confirm this. Alternatively, the damage loci may consist of initial disorder/amorphization rather than breaks. The damage lines are dark, possibly because there is no significant separation between the fractured surfaces. Breaks in nanotubes were rarely observed previously following specimen cutting,[9,12] which was taken to imply that nanotubes have very high strength.[8] The fragmentation phenomenon observed here is, therefore, due to either (i) compressive thermal residual stresses resulting from polymer shrinkage during polymerization, or (ii) tensile stresses generated by polymer deformation, and transmitted to the nanotube during the fragmentation experiment. Regarding hypothesis (i) above, compressive thermal residual stresses are calculated[17] to be $\sim$3.9 GPa, assuming a temperature gradient of 35 °C between the polymerization and room temperatures (60 and 25 °C, respectively), a 1.8 TPa Young's modulus for the nanotube[3] (assuming that the compressive and tensile moduli are approximately identical), and a film thickness of 200 μm. Such compressive stress would not be likely to result[18–21] in the breakage of 1–5 μm long nanotubes (assuming a Weibull shape parameter range of $\sim$2–3 for the nanotube, similar to high modulus graphite fibers[19]). Indeed, extensive TEM examination yielded no breaks or nanotube fragmentation in

[a]Corresponding author. Electronic mail: cpwagner@wis.weizmann.ac.il

 0003-6951/98/72(2)/188/3/$15.00

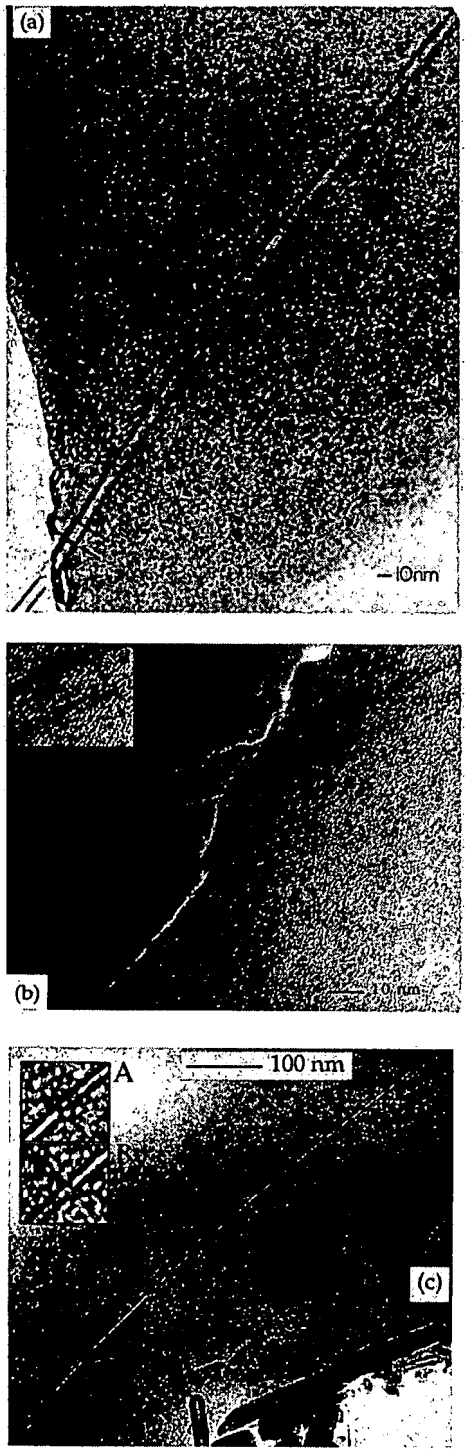

FIG. 1. (a) TEM picture of a multilayer carbon nanotube at the polymer film boundary, revealing the extent of nanotube fragmentation (arrows). Electron diffraction by the polymer material strongly weakens the contrast between the nanotube and the surrounding matrix. (b) Higher magnification view of (a). Two nanotube breaks are visible (arrows). These are either due to the specimen deformation under stress, or possibly to extraneous bending stresses. (c) Low magnification TEM picture of a multiwall nanotube in the polymer film, showing nanotube fragmentation (arrows).

the specimens that had not been subjected to a prior mechanical deformation. Since nanotube fragmentation is observed in stressed specimens, we conclude that it is due mostly to the large stress induced in the nanotube during

TABLE I. Carbon nanotube fragmentation data.

Nanotube fragment No.	Inner diameter (nm)	Outer diameter (nm)	Fragment length (nm)
1	4.2	16.6	210.8
2	4.2	16.6	348.6
3	3.2	10.8	115.6
4	3.2	10.8	226.8
5	4.2	8.4	46.2
6	4.2	8.4	88.2
7	3.3	10.9	436.0
8	3.3	10.9	218.0
9	5.5	11.1	157.3
10	5.5	11.1	207.2

tensile testing of the films. Indeed, using a simple isostrain elastic model, this stress is of the order of $\sigma_{NT} = (E_{NT}/E_m)\sigma_m \approx 55$ GPa, where Young's moduli of the nanotubes and the polymer matrix are $E_{NT} = 1.8$ TPa and $E_m = 2$ GPa, respectively, and the applied matrix stress is $\sigma_m = 60$ MPa.

Fragment length measurements were performed using several sets of TEM pictures and the resulting data are included in Table I. We assumed that these lengths were those measured at the saturation limit in the fragmentation experiment, when additional nanotube breakage is prevented because the applied stress in progressively shorter fragments eventually cannot overcome their increasingly higher strength. The normalized fragment length, l_c/D_{NT}, of nanotubes falls within the range 5–20. For comparison, the normalized fragment length obtained in single-fiber fragmentation tests performed using high-modulus pitch-based graphite fibers,[19] using the same UV-curable polymer as the matrix, is about 50. The normalized fragment length appears to further increase as the Young's modulus decreases, Table II.

Assuming that the applied stress is transferred to the nanotube via a nanotube-matrix interfacial shear mechanism at the molecular level, a force balance-based expression for the nanotube–polymer interfacial shear strength τ_{NT} may be derived as follows:

$$\tau_{NT} = \left(\frac{\sigma_{NT}(l_c)}{2(l_c/D_{NT})}\right)\left(1 - \frac{d_{NT}^2}{D_{NT}^2}\right), \tag{1}$$

where $\sigma_{NT}(l_c)$ is the strength of a nanotube fragment of length l_c (the saturation length), and d_{NT} and D_{NT} are the inner and outer tube diameters, respectively. Equation (1) is a simple generalization of the classical model of Kelly and Tyson,[22] to which it reduces for the case of full tubes ($d_{NT} = 0$). The case of single-wall nanotubes is obtained when $d_{NT} \to D_{NT}$. With the values of d_{NT}/D_{NT} found here, the second factor in the right-hand side of Eq. (1) is 0.75–0.90, but should become significantly smaller for thinner-wall nanotubes. Thus, the determining parameter in Eq. (1) is the tensile strength $\sigma_{NT}(l_c)$ of nanotube fragments of length l_c. There is currently no simple way to measure this. However, recent experiments[23] provide estimates of about 150 GPa for the *compressive* strength of multiwall carbon nanotubes. For strong fibers used in the composite materials field,[19–21] the ratio of compressive-to-tensile strength is 0.1–0.3, and if the

TABLE II. Fragmentation data for low- (LM), medium- (MM), and high-modulus (HM) graphite fibers.

Fiber diameter[a] D (μm)	Elastic modulus[a] (GPa)	Interface shear strength,[b] τ_i (MPa)	Fragment aspect ratio at saturation, l_c/D
9.9	250 (LM)	8.3	108.3
9.8	400 (MM)	13.5	61.9
9.5	750 (HM)	43.3	48.8

[a]Data from Ref. 19.
[b]Calculated by means of a force balance model (Ref. 18).

same applies to carbon nanotubes, tensile strengths of the order of several hundred GPa may indeed be attained, as recently speculated.[24] This, however, would be above the values of the applied stress obtained by the isostrain elastic model, as outlined earlier. (Note also that the strength of graphite whiskers measured by Bacon[25] was 20 GPa.) The ratio of compressive-to-tensile strength may, however, be closer to 1 in the case of more perfect microstructures such as those of nanotubes. Using 50 GPa as a conservative value in Eq. (1), we find that the stress transfer ability τ_i of nanotubes–polymer interfaces is of the order of 500 MPa and up, thus, an order of magnitude higher than the stress transfer ability of current advanced composites. An increase of τ_i with Young's modulus is also observed in graphite fibers, see Table II. In other words, it is most probable that such interfaces are more able than either the matrix, or the nanotubes themselves, to sustain shear. This might explain our observation of "telescopic" ruptures in multiwall carbon nanotubes (Fig. 2).

A fundamental question arises regarding the nature (at the molecular scale) of the stress transfer mechanism in nanotube-based composites. Interfacial energies normally amount to[26] $\sim 50-300\ \mathrm{J/m^2}$ when chemical bonds are present and to the $50-350\ \mathrm{mJ/m^2}$ range[27] if only van der Waals forces are assumed. The weaker fiber–polymer interfacial strength, as compared to the nanotube–polymer interfacial strength, can possibly be explained by the presence, at the interface, of much larger defects that facilitate the propagation of an interfacial crack. The higher strength of nanotube–polymer interfaces may, in fact, arise from a mechanism similar to the "2+2" cycloaddition reaction demonstrated for C_{60} photopolymerization.[13,14] The strong curvature, as well as the presence of multiple concentric graphene planes, are likely to strongly enhance the reactivity of carbon nanotubes towards double-bonds containing polymeric chains, upon UV curing of the specimens.

An additional minor stress transfer mechanism is possible as well, namely, that the macroscopic stress is also transferred in tension through the nanotube ends. This may arise from the increased polymer–tube affinity due to the presence of graphite pentagonal defects at the tube end caps. This, however, is difficult to verify at this point. The effect of other structural parameters, such as wall thickness or helicity,[2,8] on the nanotube strength remains to be studied. We are planning to perform experiments to verify whether single-wall nanotubes exhibit significantly different fragmentation behavior.

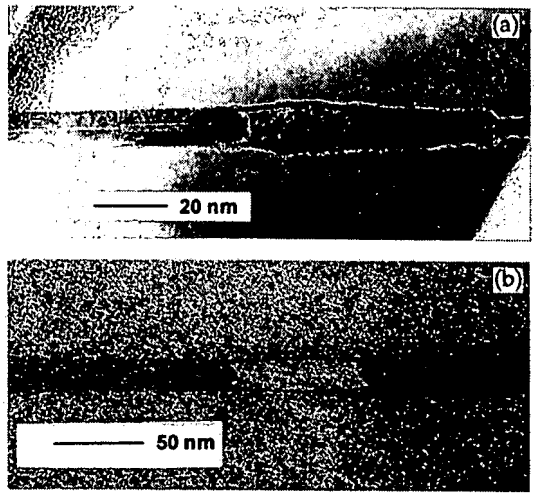

FIG. 2. Examples of telescopic rupture of a multiwall nanotube in the polymer film. Note the intact wall–polymer interface, contrasting with the longitudinal rupture in shear of the internal wall structure [this is especially evident in photograph (a) above].

[1] J. F. Despres, E. Daguerre, and K. Lafdi, Carbon **33**, 87 (1995).
[2] S. Iijima, C. Brabec, A. Maiti, and J. Bernholc, J. Chem. Phys. **104**, 2089 (1996).
[3] M. M. J. Treacy, T. W. Ebbesen, and J. M. Gibson, Nature (London) **381**, 678 (1996).
[4] G. Overney, W. Zhong, and D. Tomanek, Z. Phys. D **27**, 93 (1993).
[5] D. H. Robertson, D. W. Brener, and J. W. Mintmire, Phys. Rev. B **45**, 12 592 (1992).
[6] N. G. Chopra, L. Benedict, V. Crespi, M. Cohen, S. Louie, and A. Zettl, Nature (London) **377**, 135 (1995).
[7] J. M. Molina, S. S. Savinsky, and N. V. Khokhriakov, J. Chem. Phys. **104**, 4652 (1996).
[8] B. I. Yakobson, C. J. Brabec, and J. Bernholc, Phys. Rev. Lett. **76**, 2511 (1996).
[9] P. M. Ajayan, O. Stephan, C. Colliex, and D. Trauth, Science **265**, 1212 (1994).
[10] P. Calvert, Nature (London) **357**, 365 (1992).
[11] T. W. Ebbesen, Annu. Rev. Mater. Sci. **24**, 235 (1994).
[12] P. M. Ajayan, Condens. Matter News **4**, 9 (1995).
[13] A. M. Rao and P. C. Eklund, in *Cluster Assembled Materials, Materials Science Forum*, edited by Klaus Sattler (Trans. Tech., Switzerland, 1996), Vol. 232, pp. 173–206.
[14] A. M. Rao, P. Zhou, K.-A. Wang, G. T. Hager, J. M. Holden, Y. Wang, W.-T. Lee, X.-X. Bi, P. C. Eklund, D. S. Cornett, M. A. Duncan, and I. J. Amster, Science **259**, 955 (1993).
[15] H. D. Wagner and A. Eitan, Appl. Phys. Lett. **56**, 1965 (1990).
[16] I. J. Beyerlein and S. L. Phoenix, Compos. Sci. Technol. **56**, 75 (1996).
[17] H. D. Wagner, Phys. Rev. B **53**, 5055 (1996).
[18] J. R. Wood, H. D. Wagner, and G. Marom, Proc. R. Soc. London, Ser. A **452**, 235 (1996).
[19] H. D. Wagner, J. Aronhime, and G. Marom, Proc. R. Soc. London, Ser. A **428**, 493 (1990).
[20] G. J. Hayes, D. D. Edie, and J. M. Kennedy, J. Mater. Sci. **28**, 3247 (1993).
[21] T. Ohsawa, M. Miwa, M. Kawade, and E. Tsushima, J. Appl. Polym. Sci. **39**, 1733 (1990).
[22] A. Kelly and W. R. Tyson, J. Mech. Phys. Solids **13**, 329 (1965).
[23] O. Lourie, D. M. Cox, and H. D. Wagner (unpublished).
[24] B. I. Yakobson and R. E. Smalley, Am. Sci. **85**, 324 (1997).
[25] R. Bacon, J. Appl. Phys. **31**, 283 (1960).
[26] A. T. DiBenedetto, Compos. Sci. Technol. **42**, 103 (1991).
[27] M. Nardin and J. Schultz, J. Mater. Sci. Lett. **12**, 1245 (1993).

ADVANCED MATERIALS

[1] a) Y. Einaga, O. Sato, T. Iyoda, A. Fujishima, K. Hashimoto, *J. Am. Chem. Soc.* **1999**, *121*, 3745. b) S. Bénard, A. Léaustic, E. Rivière, P. Yu, R. Clément, *Chem. Mater.* **2001**, *13*, 3709. c) K. Nakatani, P. Yu, *Adv. Mater.* **2001**, *13*, 1411. d) S. Bénard, E. Rivière, P. Yu, K. Nakatani, J. F. Delouis, *Chem. Mater.* **2001**, *13*, 159. e) K. Hamachi, K. Matsuda, T. Itoh, H. Iwamura, *Bull. Chem. Soc. Jpn.* **1998**, *71*, 2973. f) K. Matsuda, M. Irie, *J. Am. Chem. Soc.* **2000**, *122*, 7195. g) D. A. Pejakovic, J. L. Manson, J. S. Miller, A. J. Epstein, *J. Appl. Phys.* **2000**, *87*, 6028.

[2] H. Tachibana, T. Nakamura, M. Matsumoto, H. Komizu, E. Manda, H. Niino, A. Yabe, Y. Kawabata, *J. Am. Chem. Soc.* **1989**, *111*, 3080.

[3] J.-C. Chiang, A. G. MacDiarmid, *Synth. Met.* **1986**, *13*, 193.

[4] For examples, see: a) G. Venugopal, X. Quan, G. E. Johnson, F. M. Houlihan, E. Chin, O. Nalamasu, *Chem. Mater.* **1995**, *7*, 271. b) S.-Z. Li, M.-X. Wan, *Chin. J. Polym. Sci.* **1997**, *15*, 108.

[5] a) F. M. Raymo, S. Giordani, *J. Am. Chem. Soc.* **2001**, *123*, 4651. b) F. M. Raymo, S. Giordani, *Org. Lett.* **2001**, *3*, 3475. c) F. M. Raymo, R. J. Alvarado, S. Giordani, M. A. Cejas, *J. Am. Chem. Soc.* **2003**, *125*, 2361. d) X. Guo, D. Zhang, Y. Zhou, D. Zhu, *Chem. Phys. Lett.* **2003**, *375*, 484. e) X. Guo, D. Zhang, Y. Zhou, D. Zhu, *J. Org. Chem.* **2003**, *68*, 5681.

[6] For examples, see: a) K. Uchida, M. Saito, A. Murakami, S. Nakamura, M. Irie, *Adv. Mater.* **2003**, *15*, 121. b) H. Tian, B. Chen, H, Tu, K. Müllen, *Adv. Mater.* **2002**, *12*, 918. c) T. B. Norsten, N. R. Branda, *Adv. Mater.* **2001**, *13*, 347. d) T. B. Norsten, N. R. Branda, *J. Am. Chem. Soc.* **2001**, *123*, 1784. e) E. Murguly, T. B. Norsten, N. R. Branda, *Angew. Chem. Int. Ed.* **2001**, *40*, 1752. f) G. M. Tsivgoulis, J. M. Lehn, *Angew. Chem. Int. Ed.* **1995**, *34*, 1119. g) L. Eggers, V. Buss, *Angew. Chem. Int. Ed.* **1997**, *36*, 881.

[7] For the present studies a mixture of polyaniline/camphorsulfonic acid (PANI/CSA) in *m*-cresol (3.7 %) and polyaniline/dodecylbenzene sulfonic acid (PANI/DBSA) in chloroform (1.0 %) at a volume ratio of 1:4 was used because: 1) for the simple preparation of the thin film by the dip-coating method, a volatile solvent like $CHCl_3$ was desirable. However, the thin-film conductivity of PANI/DBSA was low; 2) although the electrical conductivity of PANI/CSA is high, the boiling point of *m*-cresol is too high for it to be easily evaporated. Both PANI/CSA and PANI/DBSA were prepared following the reported procedures: a) Y. Cao, P. Smith, A. J. Heeger, *Synth. Met.* **1992**, *48*, 91. b) Y. Li, M. Wan, *J. Funct. Polym.* **1998**, *11*, 194.

[8] This absorption band was blue-shifted by about 50 nm relative to the corresponding band of the thin film.

[9] J. A. Osaheni, S. A. Jenekhe, H. Vanherzeele, J. S. Meth, Y. Sun, A. G. MacDiarmid, *J. Phys. Chem.* **1992**, *96*, 2830.

[10] a) S. Stafström, J. L. Brédas, A. J. Epstein, H. S. Woo, D. B. Tanner, W. S. Huang, A. G. MacDiarmid, *Phys. Rev. Sci.* **1987**, *59*, 1464. b) See ref. 7b.

[11] After being mixed with SP, the thin-film conductivity of polyaniline (PANI/CSA and PANI/DBSA) was reduced.

Carbon Nanotube Film Sensors**

By *Zhiling Li*, *Prasad Dharap*, *Satish Nagarajaiah*,* *Enrique V. Barrera*, and *Jong Dae Kim*

Since their discovery,[1] carbon nanotubes have been investigated extensively. Several experiments[2–4] have demonstrated the potential of single-walled carbon nanotubes (SWCNTs) as strain/stress sensors by relating the strain/stress of the nanotube to the Raman band shift. The electronic bandgap changes have been computed as a function of axial compression, tension stretch, torsion, and bending strain.[5–7] It has been possible to develop nanoelectromechanical sensors because of the strong dependence of the SWCNTs' band structure on the mechanical deformation. SWCNTs exhibit excellent mechanical and electrical properties. Most of the studies to date relate the mechanical deformation with the change in electrical properties at the nanoscale. The main objective of this study is to use the strain-sensing capability at the nanoscale to develop macroscale strain sensors. We propose the use of carbon nanotube films that possess isotropic properties due to the random orientation of SWCNTs; such films could be applied to structural surfaces, e.g., the skin of an aircraft wing, to measure strain at the macroscale.

It is difficult to use Raman spectroscopy for strain measurements at the macroscale in the field. The use of conventional electrical resistance strain gauges is limited to discrete points and fixed directional strain sensing. We propose the use of external probes to measure strain by contact with carbon nanotube films; the probes can easily be moved to different directions or locations, imparting the ability to sense multidirectional and multiple-location strain at the macroscale. Additionally, the strain gauges are separate from the material, not embedded. Carbon nanotube films can be integrated into the material, for example in composites, and hence can function both as sensors and as the structural material. We demonstrate here that carbon nanotube films can be used to measure strain at the macroscale.

[*] Prof. S. Nagarajaiah, Z. Li, P. Dharap
Department of Civil and Environmental Engineering and
Department of Mechanical Engineering and Material Science
Rice University
Houston, TX, 77005 (USA)
E-mail: nagaraja@rice.edu
Prof. E. Barrera
Department of Mechanical Engineering and Materials Science
Rice University
Houston, TX, 77005 (USA)
J. D. Kim
Department of Chemical Engineering
Rice University
Houston, TX, 77005 (USA)

[**] The authors wish to acknowledge the support of the Texas Institute for Intelligent Bio-Nano Materials and Structure for Aerospace Vehicles, funded by NASA Cooperative Agreement No. NCC-1-02038.

  DOI: 10.1002/adma.200306310

Several experiments have demonstrated the potential of SWCNTs in composites as nanoscale sensors.[2-4] The Raman band of SWCNTs in a polymer matrix at about 2630 cm^{-1} has been studied as a function of tensile strain[3] and the Raman band of SWCNTs in composites at about 1590 cm^{-1} has also been studied.[2] Both these studies have shown that the shift in the Raman modes is a function of the strain applied to the SWCNTs. As a first step, we demonstrate that carbon nanotube films are Raman-active and can be used to sense strain.

In order to produce the carbon nanotube films, unpurified SWCNTs from Carbon Nanotechnologies Incorporated (CNI) were mixed with 0.25 mg/mL *N,N*-dimethylformamide (DMF) and the mixture was filtered through a 0.2 mm Teflon membrane. After rinsing and drying of the remaining material, freestanding carbon nanotube films (buckypapers) were peeled from the filter. Then, the films were dried for 24 h under vacuum. Figures 1a,b show scanning electron microscopy (SEM) pictures of a carbon nanotube film with 30 μm thick-

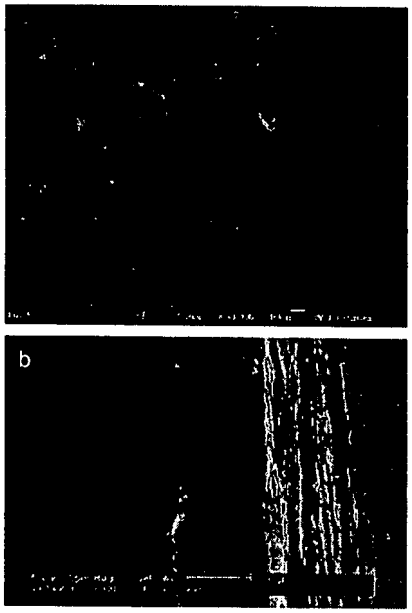

Figure 1. SEM images of a carbon nanotube film: a) plan view showing randomly distributed bundles of SWCNTs in a carbon nanotube film (scale 100 nm); b) cross-section of the carbon nanotube film (scale 20 μm).

ness. It can be seen that the film is made up of randomly oriented bundles of SWCNTs. To study the effectiveness of the film in measuring strain, it was attached to a rubber strip, using high strength epoxy to ensure perfect bonding. The rubber strip was loaded with tensile forces in order to induce axial tensile strains in the film, and the corresponding Raman spectra were recorded. A conventional strain gauge was attached to the other side of the rubber specimen to measure the strain transferred to the nanotube film.

Polarized Raman measurements were performed at room temperature using a Renishaw Raman microscope. Ar^+ (514.5 nm, 2.41 eV) laser light was used and the readings were recorded in the back-scattering configuration. As concluded by Frogley et al.,[3] when using polarized light, randomly oriented nanotubes can be used as strain sensors so that no fixed nanotube alignment is necessary and strains can be measured in all directions in a single sample. The exciting laser spot was kept at the same position throughout the experiment and the polarized laser was kept parallel to the direction in which the axial tension was applied.

It can be seen from Figure 2a that the Radial Breathing (RB) modes[2,8] are not affected by the strains in the film. The peaks remain unchanged as the axial tensile strains are increased from 0.03 % to 0.094 %. However, for the correspond-

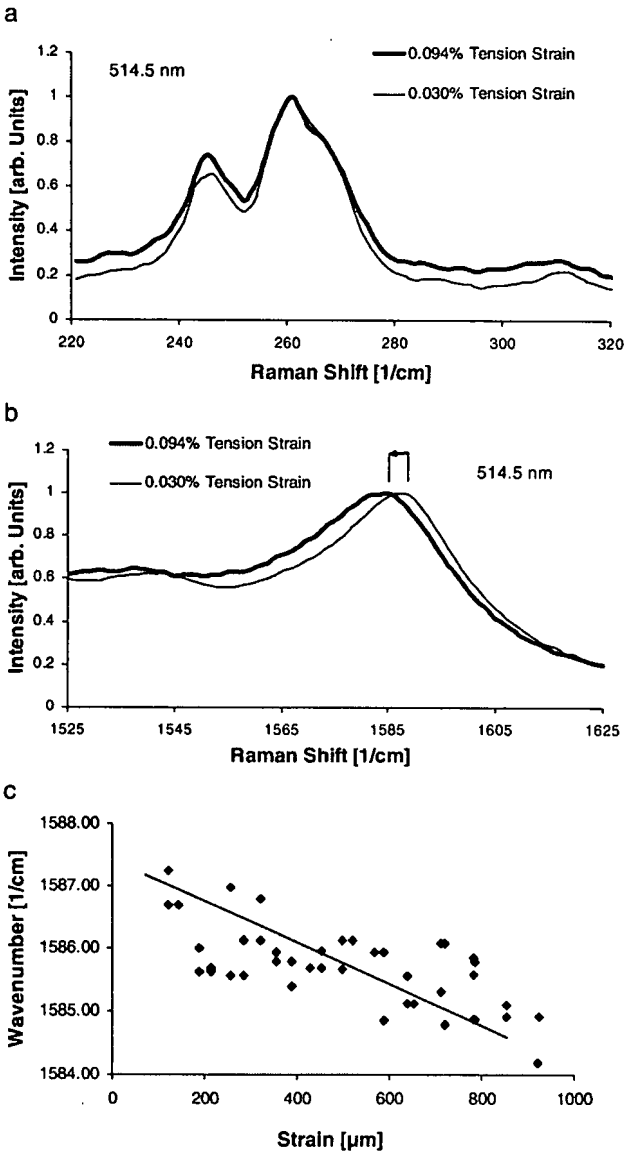

Figure 2. Raman spectra of the carbon nanotube film: a) RB modes; b) shift in G-band modes; c) the G-band peak position for SWCNTs in the carbon nanotube film, as a function of tensile strain.

ADVANCED MATERIALS

ing change in strains, the peak of the G band (C–C stretching tangential modes) shifts downwards by about 2 cm^{-1}, as shown in Figure 2b. The D band, at 2654 cm^{-1}, is rather complicated to interpret[2,9] because of the mode dispersion involved in the scattering process, and is therefore not considered in this study.

The Raman wavenumber shift of the G band of carbon nanotube films as a function of tensile strain is shown in Figure 2c. From this figure it can be seen that the Raman wavenumber of the G modes shifts downward when the tensile strain in the film increases. Although the data are scattered, the downward trend is clear—the solid line is the linear regression of the data. It can be concluded that there is a relationship between the tensile strains applied to the carbon nanotube films and the G band mode peak from the Raman spectroscopy study.

The Raman shift confirms that nanotubes are strained due to axial tensile strain on the carbon nanotube film. The strain in the nanotubes alters its electrical properties,[5–7] hence carbon nanotube films can be used as strain sensors.

The elaborate setup needed for Raman spectroscopy makes it less practical for field applications such as measuring the strain in an aircraft wing. Therefore, a movable four-point probe was proposed to measure the change in voltage across the carbon nanotube film due to tensile strain. A carbon nanotube film was attached to a 12 in. × 1.5 in. × 0.065 in. (1 in. = 2.54 cm) brass specimen, with poly(vinyl chloride) (PVC) between the brass specimen and film for insulation. The Young's modulus of the brass specimen is 96 GPa. High-strength epoxy and a vacuum-bonding method were applied to ensure perfect strain transfer between the brass, PVC, and film. A conventional electrical resistance strain gauge was attached to the other side of the specimen to measure the strain. The specimen was subjected to tensile force using a servohydraulic machine and the corresponding change in voltage was measured using a four-point probe measurement.[10] Four colinear copper probes spaced at 0.3 in. center to center were used for the four-point-probe measurement. The input current across the two outer probes was kept constant during the measurement and the change in voltage across the two inner probes was measured.

Figure 3 shows the voltage changes in the carbon nanotube film as a function of the measured tensile strain from the conventional gauge. As the tensile strain measured by the conventional gauge increases from 0–1000 μm/m the voltage changes measured across the two inner probes increase by nearly 350 μV. There is a linear relationship between the change in voltage and the strain, although the data are scattered and further investigation is needed. The change in voltage was measured by moving the four-point probe to several parallel locations, in line with the axial forces on a single carbon nanotube film; this also yielded a linear trend.

The change in voltage between the inner two probes comes from two sources: 1) the change of resistivity in the nanotube film, and 2) dimension changes of the nanotube film. Since in this experiment the strains of the brass specimen are of the order of 0.1 %, the changes in the dimensions of the film will be small, and therefore their contributions to the change in voltage will also be small, as demonstrated below. The film resistivity ρ is given by[10]

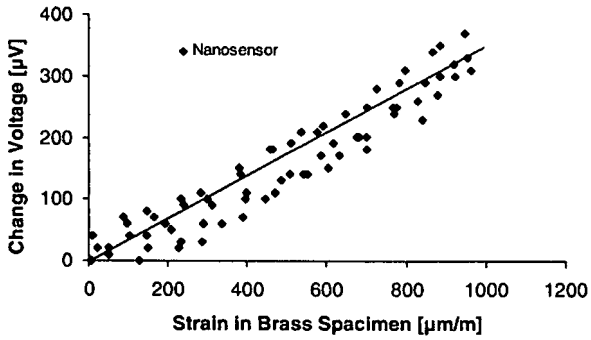

Figure 3. Brass specimen, with a carbon nanotube film attached to it, subjected to tension: strain as a function of change in voltage in the carbon nanotube film.

$$\rho = \frac{V}{I} C\left(\frac{a}{d}, \frac{d}{s}\right) \quad (1)$$

where V is the voltage across the inner two probes, I is the constant input current across the outer two probes, and C is a factor dependent on the length (a), width (d), and distance (s) between the probes. If the resistivity of the nanotube film is assumed to be constant, the change in voltage due to the dimension change can be obtained by

$$\Delta V = \rho I\left(\frac{1}{C_2} - \frac{1}{C_1}\right) = 32\ (\mu V) \quad (2)$$

where C_1 (1.94645) and C_2 (1.94586) are the factors[10] depending on the change of dimensions of the nanotube film due to tensile strain, and the input current is constant at 107.5 mA. From the above equations the change in voltage corresponding to the change in tensile strain from 0 to 0.1 % is 32 μV. From Figure 3 the measured change in voltage across the inner two probes is 350 μV for 0.1 % tensile strain. From the above analysis it is clear that the change in voltage due to the dimension change of the nanotube film is small (9 %) and hence the change in voltage is mainly related to the change in resistivity (91 %).

In conclusion, a carbon nanotube film can be used as a strain sensor at the macroscale, due to the dependence of the electrical properties of SWCNTs on mechanical deformation at the nanoscale. In addition, carbon nanotube films are made up of randomly oriented SWCNTs, so their electronic properties are independent of direction. Hence, taking measurements along different directions will provide the corresponding strains.[11] Carbon nanotube films made up of aligned SWCNTs can be expected to be more sensitive to tensile strains than carbon nanotube films made up of randomly oriented SWCNTs, although further research is needed. The results presented in this paper demonstrate the potential of carbon nanotube films in measuring strain at the macroscale.

Experimental

Nanotube films made of unpurified SWCNTs from CNI were attached to a rubber specimen. The G-band and RB mode shift in the carbon nanotube films were measured on a Renishaw Raman microscope as the rubber specimen was subjected to a tensile force. The corresponding strain in the carbon nanotube film was measured by conventional strain gauges attached to the other side of the rubber specimen.

Carbon nanotube films were attached to the brass specimen using high-strength epoxy combined with a vacuum bonding method. Conventional strain gauges were attached to the opposite side of the brass specimen. A four-point-probe method was used to measure the voltage across the inner two probes with a constant current passing through the outer two probes. The brass specimen was subjected to tensile forces on an Instron 5586 servo hydraulic test frame.

Received: October 12, 2003
Final version: December 25, 2003

[1] S. Iijima, *Nature* **1991**, *318*, 162.
[2] V. G. Hadjiev, M. N. Iliev, S. Arepalli, P. Nikolaev, B. S. Files, *Appl. Phys. Lett.* **2001**, *78*, 3193.
[3] M. D. Frogley, Q. Zhao, H. D. Wagner, *Phys. Rev. B* **2002**, *65*, 113413.
[4] Q. Zhao, J. R. Wood, H. D. Wagner, *Appl. Phys. Lett.* **2001**, *78*, 1748.
[5] L. Yang, J. Han, *Phys. Rev. Lett.* **2000**, *85*, 154.
[6] T. W. Tombler, C. Zhou, L. Alexseyev, J. Kong, H. Dai, L. Liu, C. S. Jayanthi, M. Tang, S. Y. Wu, *Nature* **2000**, *405*, 769.
[7] S. Peng, L. Cho, *J. Appl. Mech.* **2002**, *69*, 451.
[8] A. M. Rao, E. Richter, S. Bandow, B. Chase, P. C. Eklund, K. A. Williams, S. Fang, K. R. Subbaswamy, M. Menon, A. Thess, R. E. Smalley, G. Dresselhaus, M. S. Dresselhaus, *Science* **1997**, *275*, 187.
[9] R. Saito, G. Dresselhaus, M. S. Dresselhaus, *Physical Properties of Carbon Nanotubes*, Imperial College Press, London **1998**.
[10] F. M. Smits, *Bell Syst. Tech. J.* **1959**, *5*, 711.
[11] P. Dharap, Z. Li, S. Nagarajaiah, E. V. Barrera, *Nanotechnology* **2004**, *15*, 379.

Reversible Diastereoselective Photocyclization of Diarylethenes in a Bulk Amorphous State

By *Tadatsugu Yamaguchi*,* *Kazuko Nomiyama*, *Munetoshi Isayama*, and *Masahiro Irie*

Diarylethene derivatives are very promising photochromic compounds for application as optoelectronic devices because of their fatigue resistant and thermally irreversible performance.[1,2] One of the characteristic properties of the diarylethenes is that the colored closed-ring isomers have chiral carbon atoms. Upon irradiation with ultraviolet light, colorless open-ring isomers are converted to enantiomers (*R,R* and *S,S*) of the closed-ring isomers.

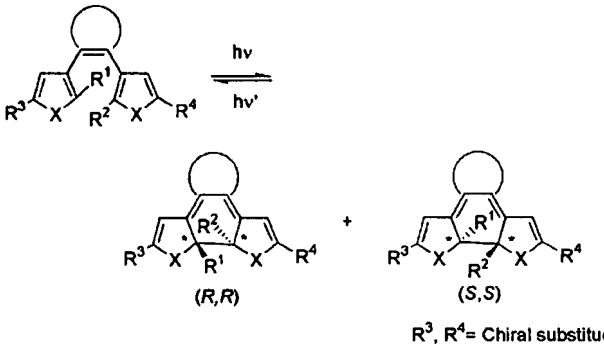

R^3, R^4= Chiral substituent

Various attempts have been carried out to enrich one of the enantiomers (or diastereomers),[3–7] because optical rotation changes by photoirradiation are potentially useful for nondestructive readout in optical memories.

For practical applications, photochromic reactions should take place in solid matrices. Although successful enrichment of one of the diastereomers was observed in crystals of a diarylethene with a chiral substituent,[4] the crystalline state is hard to process. A bulk amorphous state is favorable for processing and has various advantageous characteristics for practical usage, such as high dye density and high optical transparency.[8–10] In this communication we report on an asymmetric induction in the photochromic reactions of diarylethene derivatives **1a**, **2a**, and **3a** in the amorphous state.

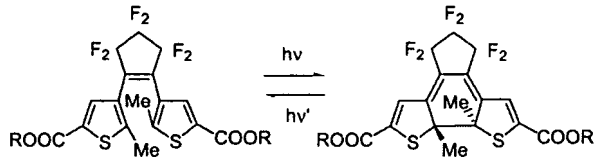

1: R=(*S*)-*sec*-butyl
2: R=(*R*)-sec-butyl
3: R=*l*-menthyl

1a-3a **1b-3b**

Diarylethenes **1a–3a**, which have two chiral units, were synthesized by carboxylation of the 1,2-bis(2-methyl-5-bromothiophen-3-yl)perfluorocyclopentene **4**,[11] which is prepared by bromination of 1,2-bis(2-methyl-thiophen-3-yl)perfluorocyclopentene in tetrahydrofuran (THF),[12] and successive esterification of the carboxylic acid with (*S*)-2-butanol, (*R*)-2-butanol, *l*-menthol.[13–15]

Upon irradiation with UV light in hexane solution, compounds **1a–3a** underwent photocyclization reactions to give two diastereomers. These diastereomers were isolated by high performance liquid chromatography (HPLC) performed with a silica gel column (Wakosil 5SIL), using hexane/ethyl acetate as an eluent, and the electronic absorption spectra of the two diastereomers were measured.[13–15] Because the two closed-ring diastereomers showed the same absorption maximum

[*] Dr. T. Yamaguchi, K. Nomiyama, Dr. M. Isayama
Fukuoka Industrial Technology Center
Kamikoga 3-2-1, Chikushino, Fukuoka, 818-8540 (Japan)
E-mail: tyama@fitc.pref.fukuoka.jp
Prof. M. Irie
Department of Chemistry and Biochemistry
Graduate School of Engineering, Kyushu University
Hakozaki 6-10-1, Higashi-ku, Fukuoka, 812-8581 (Japan)

DOI: 10.1002/adma.200305815

Raman scattering test of single-wall carbon nanotube composites

V. G. Hadjiev[a)]
Institute for Space Systems Operations and Texas Center for Superconductivity, University of Houston, Houston, Texas 77204

M. N. Iliev
Texas Center for Superconductivity, University of Houston, Houston, Texas 77204

S. Arepalli and P. Nikolaev
G. B. Tech./Lockheed Martin, 2400 NASA Road One, Mail Stop C61, Houston, Texas 77058

B. S. Files
NASA Johnson Space Center, Houston, Texas 77058-3696

(Received 17 August 2000; accepted for publication 27 March 2001)

Raman spectroscopy is used to infer elastic properties of single-wall carbon nanotubes (SWNTs) in composites. This letter presents strain-induced frequency shift of tangential Raman active modes of SWNTs embedded in epoxy resin subjected to bending. Epoxy curing and sample extension in the tensile strength test are found to create residual strains on the SWNT ropes. We demonstrate that specimen compression in combination with the Raman microprobe technique provides a means for determining of these strains and hence load transfer effectiveness. © *2001 American Institute of Physics.* [DOI: 10.1063/1.1373405]

Single-wall nanotubes (SWNTs) are believed to be the ultimate reinforcement material in polymer composites, due to their high aspect ratio (up to 10^4), Young's modulus ($\sim 10^3$ GPa) close to that of diamond,[1] tensile strength of ~ 50 GPa,[2] and light weight (density of ~ 1.3 g/cm^3).[3] In practice, preparation of high strength nanocomposites has yet to overcome several obstacles. SWNTs form different diameter crystalline nanoropes that usually exhibit bends and loops.[1] As the rope diameter increases, shear deformation reduces the effective moduli of nanoropes by an order of magnitude with respect to that of a SWNT.[4] Therefore, controllable dispersion and alignment of SWNTs in composites are desirable to achieve improvement of the mechanical properties. In addition, interface region properties are known to be crucial for load sharing between the matrix and the reinforcement material.[5] There is little knowledge of the interface region in nanocomposites since direct studies[2,4] are obstructed by the nanosize diameter and high aspect ratio of a SWNT/rope.

In this letter, we report an application of Raman spectroscopy for nondestructive studies of residual strains and load transfer in nanocomposites. The few reports[6] on the application of Raman spectroscopy to nanocomposites have dealt with the second order D^* band at ~ 2650 cm^{-1}. However, this Raman band is rather complicated to interpret because of the modes dispersion involved in the scattering process.[1] Instead, we focus our study on the graphite-like carbon vibrations at ~ 1590 cm^{-1}. These modes have been studied in detail by several theoretical approaches.[1]

SWNTs produced by laser ablation[7] were purified and dispersed in Shell epon resin 862/EPI-CURE W[8] at 1 wt% loading. The epoxy-nanotube mixture was cured at 170 °C and a bar ($2\times5\times50$ mm) was prepared and cut into two specimens. The first specimen (a small piece of material) was measured as prepared ("unstressed" specimen A). Elastic properties of the second specimen were first determined by a standard tensile strength test to failure ("stressed" specimen B). For subsequent Raman measurements the B specimen was loaded in a four-point bending rig in compression to a maximum surface strain ε_s of -0.45%. Surface strain was measured by means of a 120 Ω resistance gauge. Our estimates[9] show that the top layer of the composite has experienced uniform compression. Raman spectra, excited with Ar^+ (514.5 nm) and HeNe (632.8 nm) laser lines, were recorded on a multichannel spectrometer in a backward scattering configuration with parallel incident and scattered light polarizations. The laser power density was kept less than 500 W/cm^2. The spectrometer slits were set to 2.5 cm^{-1} spectral width and absolute accuracy of 0.5 cm^{-1}. The exciting laser spot of diameter ≈ 2 μm was kept at one and the same position, close to the strain gauge, throughout the experiment. A reference epoxy-resin sample has given structureless Raman response under 514.5 nm excitation.

Figure 1 shows the low-frequency part of the Raman spectra with bands corresponding to the radial breathing type vibrations (RB modes, $A_{1(g)}$ symmetry). Within experimental accuracy, the position of the strongest band at 185 cm^{-1} (514.5 nm) does not shift in going from purified to embedded in the composite SWNTs (specimen A). The frequency of RB-modes typically increase by ~ 7 cm^{-1}/GPa under hydrostatic pressure.[10] Therefore, within experimental resolution, one may expect residual stresses of less than 70 MPa, due to epoxy shrinkage in the curing process, provided only the hydrostatic pressure effect is taken into account. We also conclude that the bands at ~ 185 cm^{-1} (514.5 nm) stem from ~ 1.3 nm diameter semiconducting nanotubes possibly of type (12,7), whereas those at ~ 170 and 191 cm^{-1} (632.8 nm) come from metallic (12,9) and (12,6) tubes, respectively.[11]

a)Electronic mail: vhadjiev@bayou.uh.edu

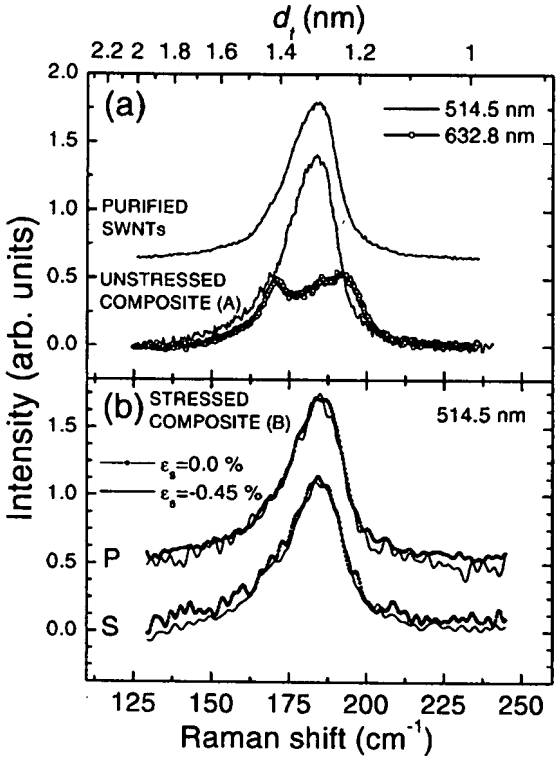

FIG. 1. Low-frequency Raman spectra of SWNTs at room temperature: (a) Spectra are measured in parallel incident and scattered light polarizations; (b) The scattering geometry is as in (a). P and S denote incident light polarizations parallel and perpendicular to the tensile stress direction, respectively. The upper horizontal scale gives the corresponding tube diameter d_t(nm)$=232/[\omega(\text{cm}^{-1})-6.5]$.

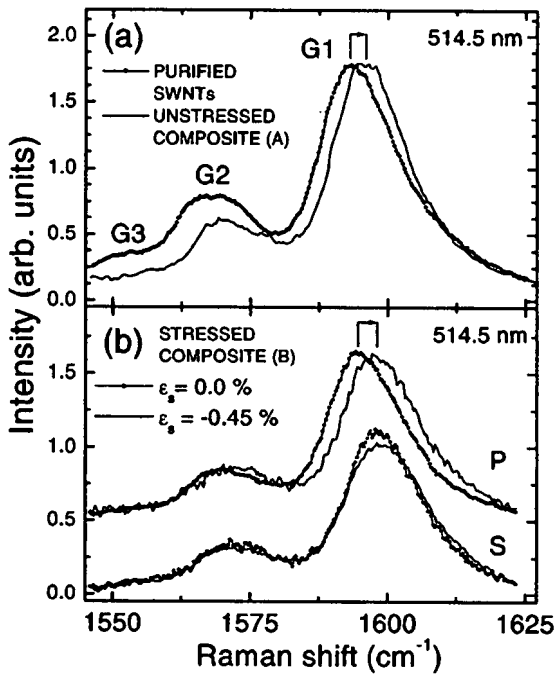

FIG. 2. High-frequency SWNTs modes measured at the same condition as in Fig. 1. The $G1$-peak position in (a) negligibly varies with the incident light polarization.

Figure 1(b) shows the RB modes in the stressed specimen B. As seen from Figs. 1(a) and 1(b), the peak position of the RB modes remains unchanged after unloading from an *extension* tensile test for the incident light polarizations parallel (P) and perpendicular (S) to the tensile stress direction. Also, no appreciable changes are seen in Fig. 1(b) upon applying compression from zero to -0.45% surface strain in the bending rig.

SWNTs modes shown in Fig. 2(a) involve tangential C–C bond stretching motions. Generically, they stem from the E_{2g_2} mode at 1580 cm^{-1} in graphite: $E_{2g_2}\rightarrow A_{1(g)}+E_{1(g)}+E_{2(g)}$.[1] Only the armchair and zig-zag SWNT modes are of even parity g. In contrast to the RB modes (Fig. 1), the graphite-like G modes in Fig. 2(a) exhibit a definite upward shift after the nanotubes were embedded in an epoxy matrix. The $G1$ band in Fig. 2(a) is composed of $A_{1(g)}$ and $E_{2(g)}$ semiconducting SWNTs, whereas those in the $G3$ band are mostly metallic.[1,12] Interestingly, the $G1/G2$-band position (specimen B) in Fig. 2(b) is different when measured for polarizations along the P and S direction. The $G1$ frequency measured for the S polarization almost coincides with that of the unstressed specimen A and does not depend on the compressive strain applied in the bending rig. In contrast, the P-polarized $G1$-peak position is closer to that in purified SWNTs and shifts upward by 3 cm^{-1} under a compressive strain of $\varepsilon_s=-0.45\%$ along the P direction. A surface strain of $\varepsilon_s=-0.40\%$ pushes up the $G1$-peak frequency to its value in the unstressed composite. We note that the Raman intensity measured in parallel polarizations is dominated by scattering from SWNTs aligned along the incident polarization direction.[1]

We summarize the experimental findings as follows: (i) The RB-band frequency does not change in going from purified SWNTs to composites, or upon applying compressive stresses; (ii) The $G1$ modes exhibit an obvious upward shift after epoxy curing; (iii) A 514.5 nm laser line excites predominately semiconducting SWNTs; (iv) Tensile stress to failure (specimen B) releases epoxy-curing-induced strain on those SWNTs that are oriented along the applied stress direction, whereas the strain on the perpendicularly aligned nanotubes remains unchanged within experimental resolution; and (v) Composite (specimen B) compression in the bending rig to $\varepsilon_s=-0.40\%$ loads the SWNTs to the strain they have in the unstressed specimen A.

From the aforementioned findings, we conclude that the observed shift of the G modes and absence of frequency change for the RB modes excludes from consideration a van der Waals type mechanism which is found to govern the RB- and G-modes shift under hydrostatic pressure.[10] Rather, it suggests a direct coupling of SWNTs/ropes to the epoxy matrix. We note that although the findings (iv) may hint at the decoupling of the SWNTs as a result of the tensile stress, those in (v) evidence more for a deformation of the matrix after the tensile test that, however, preserves SWNTs–matrix coupling. Moreover, the observed $G1$-peak shift along with the tensile test data allows us to relate the applied stress σ_c on the composite to that on the embedded SWNTs. Next, we exploit this possibility in more detail.

At equilibrium, the balance of forces requires: $\sigma_c=f\bar{\sigma}_{\text{nr}}+(1-f)\bar{\sigma}_m$, where f denotes the nanoropes volume fraction, $\bar{\sigma}_{\text{nr}}$ and $\bar{\sigma}_m$ are the volume-average nanoropes and matrix stresses, respectively. f is related to the weight frac-

tion f_{wt} as $f=f_{wt}(\rho_{nr}/\rho_m)$. Since the nanorope density ($\rho_{nr} \approx 1.3\ g/cm^3$)[3] and that of epoxy ($\rho_m=1.23\ g/cm^3$)[8] are very close, $f\approx 0.01$. We can write (Hooke's law): $\bar{\varepsilon}_c\bar{E}_c = f\bar{\varepsilon}_{nr}\bar{E}_{nr}+(1-f)\bar{\varepsilon}_m\bar{E}_m$, where $\bar{E}_c$, $\bar{E}_{nr}$, and $\bar{E}_m$ are the elastic moduli of composite, nanoropes, and epoxy material, respectively. $\bar{\varepsilon}_c=\varepsilon_s$, (Ref. 9) $\bar{\varepsilon}_{nr}$, and $\bar{\varepsilon}_m$ are the corresponding strains. The tensile test has given $\bar{E}_c=2.37$ GPa and $\bar{E}_m=2.05$ GPa. To a good approximation, $\bar{\varepsilon}_m$ is $\approx\varepsilon_s$ due to the small value of f. This leads to $\bar{\varepsilon}_{nr}\bar{E}_{nr}=0.153$ GPa for the average stress on the SWNT ropes at $\varepsilon_s=-0.45\%$.

Unidirectional stress applied on a matrix containing a single nanorope at angle ϕ to the stress direction introduces *axial* strain $\varepsilon_{nr}(\phi)=l_t\bar{\varepsilon}_m(\cos^2\phi-\nu_m\sin^2\phi)$, where ν_m is the Poisson's ratio of the matrix. The coefficient l_t denotes transfer of the strain from the matrix to the nanorope: $\varepsilon_{nr,z}=l_t\bar{\varepsilon}_m$, $0\leqslant l_t\leqslant 1$. The average nanorope strain $\bar{\varepsilon}_{nr}$ can be obtained from $\varepsilon_{nr}(\phi)$ after appropriate spacial averaging. For nanoropes that are three-dimensional (3D) randomly oriented in epoxy-resin matrix ($\nu_m\approx 1/3$)[8] averaging gives $\bar{\varepsilon}_{nr}(3D)=\varepsilon_{nr,z}/9$, whereas the corresponding expression for two-dimensional (2D), random-in-plane, distribution is $\bar{\varepsilon}_{nr}(2D)=\varepsilon_{nr,z}/3$.[13]

Next, we express the frequency change of the 1594 cm^{-1} modes with strain. Tangential vibrations of a SWNT in a nanorope remain localized on the nanotube.[1] Therefore, given the experimental findings (i–iv) we consider a SWNT under uniaxial stress. The corresponding axial strain ε_z results in a strain $\varepsilon_{ci}=-\nu_t\varepsilon_z$ along the circumference, ν_t being the Poisson's ratio of the SWNT. The ε_{ci} and ε_z strains are fully symmetric in the point group of the SWNTs but not in that of the underlaying graphene sheet. This results in a shear strain that also contributes to the frequency change.[14] We adopt the relative phonon frequency shift in the presence of strain derived in Ref. 14: $\Delta\omega^{\pm}/\omega_0=-\gamma(1-\nu_t)\varepsilon_z \mp(1/2)\gamma'(1+\nu_t)\varepsilon_z$, where γ is the Grüneisen parameter and γ' the shear strain deformation potential of a SWNT. The relative shift $\Delta\omega^{\pm}/\omega_0$ depends on the phonon eigenvector direction, and the splitting $(\Delta\omega^+-\Delta\omega^-)$ is maximal for achiral SWNTs, where $\Delta\omega^+=\Delta\omega^{A_{1g},E_{2g}}$ and $\Delta\omega^-=\Delta\omega^{E_{1g}}$. In chiral SWNTs, as those we likely probed in the Raman experiment, phonon displacements may have arbitrary directions with respect to the nanotube axis. Therefore, we observed an average shift of $\Delta\omega(1594\ cm^{-1})/\omega_0\approx-\gamma(1-\nu_t)\varepsilon_z$. From this expression and $\Delta\omega(1594\ cm^{-1})=3\ cm^{-1}$, $\gamma=1.24$,[14] and $\nu_t=0.28$,[3] one readily finds $\varepsilon_z=-0.21\%$ at an external strain $\varepsilon_s=-0.45\%$ or correspondingly $l_t=0.5$. Finally, from $\bar{\varepsilon}_{nr}\bar{E}_{nr}=0.153$ GPa, we obtain $\bar{E}_{nr}(3D)=660$ GPa and $\bar{E}_{nr}(2D)=220$ GPa, provided $\varepsilon_{nr,z}=\varepsilon_z$. The values of $\bar{E}_{nr}$ compare well with recent results on direct tensile loading of SWNT ropes.[2] This comparison gives additional support to one of the important findings reported here: load is transferred predominately along the axis of the nanorope in epoxy-based composites. It also implies that SWNTs on the circumference of a nanorope in composite carry most of the load. The latter, in combination with the random distribution of the nanoropes appear to be limiting factors for efficient reinforcement of the studied composite. At the end, we estimate the strain of the nanorope due to epoxy shrinkage. The $G1$-band shifts by $\sim 2.5\ cm^{-1}$ going from purified SWNTs to unstressed composite [Fig. 2(a)], which translates to a compressive strain of the nanorope of -0.18%, provided axial load transfer takes place.

Finally, we note that metallic SWNTs in the composite under stress are found to behave similarly to semiconducting nanotubes. The interpretation of the results for the metallic nanotubes, however, is more complicated and requires additional analysis beyond the scope of the present work.

In summary, we have presented an underlying methodology of a Raman scattering test. In combination with standard mechanical tests, this methodology allows the determination of residual strains due to matrix shrinkage, elastic properties of embedded in nanocomposite SWNTs/ropes, their dispersion, and load transfer effectiveness.

The authors thank Linda Schadler of Rensselaer Polytechnic Institute for sharing her experience and lending the authors the bending stage, and C. D. Scott of NASA JSC for the critical reading of the manuscript. This work was supported by the Institute for Space System Operations and Texas Center for Superconductivity at University of Houston.

[1] R. Saito, G. Dresselhaus, and M. S. Dresselhaus, *Physical Properties of Carbon Nanotubes* (Imperial College Press, London, 1998).
[2] M. F. Yu, B. S. Files, S. Arepalli, and R. S. Ruoff, Phys. Rev. Lett. **84**, 5552 (2000).
[3] J. P. Lu, Phys. Rev. Lett. **79**, 1297 (1997).
[4] J. P. Salvetat, G. A. D. Briggs, J. M. Bonard, R. R. Bacsa, A. J. Kulik, T. Stöckli, N. A. Burnham, and L. Forró, Phys. Rev. Lett. **82**, 944 (1999).
[5] D. Hull and T. W. Clyne, *An Introduction to Composite Materials* (Cambridge University Press, Cambridge, UK, 1996).
[6] P. M. Ajayan, L. S. Schadler, S. Giannaris, and A. Rubio, Adv. Mater. **12**, 750 (2000); C. A. Cooper and R. J. Young, J. Raman Spectrosc. **30**, 929 (1999); O. Lourie and H. D. Wagner, J. Mater. Res. **13**, 2418 (1998).
[7] S. Arepalli, P. Nikolaev, W. Holmes, and C. D. Scott, Appl. Phys. A: Mater. Sci. Process. **70**, 125 (2000).
[8] Resins and Versatics Product Technical Bulletins, Shell Chemicals (P. O. Box 2465, Houston, TX 77252, Website: www.shellchemicals.com, 1998).
[9] The upper limit for the Raman scattering volume (RSV) in our experiment was set by the depth of focus $\delta_f\approx 10\ \mu m$ of the collecting optics used. Simple calculations for a bent beam give that the strain ε_f at a depth δ_f below the surface relates to the surface strain ε_s as $\varepsilon_f=\varepsilon_s+\delta_f/R$, where R is the radius of bending. In our experiment, R of ≈ 0.5 m created $\varepsilon_s=-0.45\%$ which corresponded to $0\leqslant(\varepsilon_f-\varepsilon_s)/|\varepsilon_s|\leqslant 10^{-3}$. Therefore, ε_s represents well the *average* strain within the RSV.
[10] U. D. Venkateswaram, A. M. Rao, E. Richter, M. Menon, A. Rinzler, R. E. Smalley, and P. C. Eklund, Phys. Rev. B **59**, 10 928 (1999).
[11] The RB frequency of a nanorope is found to depend on the SWNTs diameter as $\omega(cm^{-1})=6.5+232/d_t(nm)$ (see Ref. 15). On the other hand, $d_t=d\sqrt{3(m^2+n^2+mn)}/\pi$, where $d=0.142$ nm is the nearest neighbor carbon–carbon distance (m,n) are the chiral vector components. Raman scattering from SWNTs is strongly resonant: (Refs. 1 and 12) 514.5 nm line excites mostly the semiconducting SWNTs, whereas that of 632.8 nm is more effective for excitation of the metallic nanotubes (Ref. 12). Metallic are nanotubes with $2n+m=3q$, where q is an integer (Ref. 1).
[12] M. A. Pimenta, A. Marucii, S. A. Empedocles, M. G. Bawendi, E. B. Hanlon, A. M. Rao, P. C. Eklund, R. E. Smalley, G. Dresselhaus, and M. S. Dresselhaus, Phys. Rev. B **58**, 16 016 (1998); P. M. Rafailov, H. Jantoljak, and C. Thomsen, Phys. Rev. B **61**, 16 179 (2000).
[13] $\bar{\varepsilon}_{nr}(3D)=\int_0^{\pi/2}\varepsilon_{nr}(\phi)\sin\varphi d\varphi=\varepsilon_{nr,z}(1-2\nu_m)/3$; $\bar{\varepsilon}_{nr}(2D)=(1/\pi)\int_{-\pi/2}^{\pi/2}\times\varepsilon_{nr}(\phi)d\varphi=\varepsilon_{nr,z}(1-\nu_m)/2$.
[14] S. Reich, H. Jantoljak, and C. Thomsen, Phys. Rev. B **61**, 13 389 (2000).
[15] L. Alvarez, A. Righi, T. Guillard, S. Rols, E. Anglaret, D. Laplaze, and J. L. Sauvajol, Chem. Phys. Lett. **316**, 186 (2000).